The British Journal of Radiology, 85 (2012), e891–e898

Dual-source, dual-energy multidetector CT for the evaluation of pancreatic tumours

A J CHU, MD, J M LEE, MD, Y J LEE, MD, S K MOON, MD, J K HAN, MD and B I CHOI, MD

Department of Radiology, Seoul National University Hospital, Seoul, Republic of Korea

Objective: To investigate the potential diagnostic value of dual-energy CT (DECT) with virtual non-enhanced (VNE) and iodine-only images, and to determine the optimal mixed ratio of blended images for evaluation of pancreatic diseases.
Methods: Multiphasic DECT was performed in 44 patients with focal pancreatic disease. DECT was used during the pancreatic and hepatic venous phases, and a peak kilovoltage of 120 kVp was used for both non-contrast phases. For qualitative analysis of the CT images, two radiologists assessed three image sets (VNE, iodine-only and blended images) in order to determine the acceptability of VNE in replacing true non-enhanced (TNE) images, the added value of iodine-only images and the preferred blending ratio. For quantitative analyses, the CT numbers and image noise of the pancreatic parenchyma, lesions, aorta and psoas muscle were measured. The contrast-to-noise ratio of the lesion was calculated on the pancreatic phase images. The effective radiation dose for DECT and TNE images was calculated. Statistical comparisons were made using the Friedman test, the Wilcoxon test, the paired *t*-test and repeated measures of analysis of variation with Bonferroni correction for multiple comparisons.
Results: The level of acceptance of the VNE images in replacing TNE images was 90.9%. Regarding the iodine-only images, 50% of the cases were found to have an added value. The linear-blended images with a weighting factor of 0.5 were preferred.
Conclusions: DECT was able to provide high-quality VNE images that could replace TNE images and iodine-only images showing an added value. Blended images with a weighting factor of 0.5 were preferred by the reviewers.

Received 2 June 2011
Revised 20 January 2012
Accepted 30 January 2012

DOI: 10.1259/bjr/26129418

Radiological imaging is an important component in the evaluation of pancreatic disease. CT has been the initial imaging modality of choice for evaluating pancreatic pathology [1]. Recent improvements in multidetector CT (MDCT) technology, including its improved temporal and spatial resolution, facilitate the precise timing of multiphasic imaging, and have also increased the accuracy of CT for lesion detection and characterisation in the pancreas [2]. However, there are still certain problematic imaging scenarios such as the early detection of pancreatic adenocarcinoma, detection of occult neoplasms in the setting of acute or chronic pancreatitis, accuracy of pre-operative surgical staging of pancreatic malignancy and characterisation of pancreatic cystic lesions. For example, with surgical resection, a 5-year survival rate of 20% is possible only when a pancreatic cancer is small (<2 cm diameter) and there is no peripancreatic invasion [3]. Unfortunately, however, only 10–15% of pancreatic carcinomas are in this category, resulting in an overall poor survival rate [4]. These problems could be related to the inherent, limited soft-tissue contrast of MDCT or to the limited difference in vascularity between normal parenchyma and pathological lesions. Therefore, if the contrast between pancreatic lesions and pancreatic parenchyma is improved on CT scans, we may expect improved CT performance for evaluating pancreatic disease.

For the detection of early-stage pancreatic cancers or characterisation of cystic lesions, tumour-to-pancreas contrast and lesion conspicuity or demonstration of the enhancing portion within the cystic lesions is of primary importance on CT scanning [5]. Recently several studies showing the relevance of tube voltage and lesion conspicuity have been performed and have shown the attenuation value of contrast material (iodine). The attenuation increases with the use of low-voltage X-rays owing to the increased photo-electric effect [6, 7]. However, this low-voltage technique has not been widely accepted for routine abdominal scanning because of its high noise level. With the recent development of dual-energy CT (DECT), which is equipped with two X-ray tubes and two corresponding detectors, it is possible to obtain two synchronous CT acquisitions at two different energy levels (dual-energy scanning) [8, 9]. Dual-energy acquisition techniques can allow the computation of virtual non-enhanced (VNE) images as well as the generation of pure iodine images [10]. VNE images are generated by subtracting the iodinated intravenous contrast from the soft tissue from enhanced images. The iodine map is obtained through post-processing high and low peak kilovoltage data sets. Given that the

Address correspondence to: Dr Jeong Min Lee, Department of Radiology, Seoul National University Hospital, 101 Daehangno, Jongno-gu, Seoul 110-744, Republic of Korea. E-mail: jmsh@snu.ac.kr
This study was supported by a grant from the National R&D Program for Cancer Control, Ministry for Health and Welfare, Republic of Korea (1120310).

attenuation of iodine is higher at a lower tube voltage setting, we assumed that blended images with a higher weighting factor for lower peak kilovoltage images would be able to provide better conspicuity of many pancreatic lesions. However, there have been only a limited number of studies demonstrating the results of using different weighting factors for contrast enhancement of DECT or the diagnostic value of VNE images or an iodine map in the abdomen [8, 11, 12].

Therefore, in our study, we attempted to determine whether VNE images and an iodine map could provide diagnostic value for patients with pancreatic disease. Moreover, we attempted to evaluate the effect of the weighting factor of the linear blending method on contrast enhancement, contrast-to-noise ratio (CNR) and image quality.

Methods and materials

Patient population

This study was a single-institution, retrospective review of pancreatic DECT images. This study followed the guidelines of our hospital's institutional review board and proceeded after its approval. Informed written consent was waived. 44 patients [21 male, 23 female; mean age ± standard deviation (SD) 56.82 ± 11.08 years, range 26–75 years] with suspected pancreatic solid or cystic tumours based on their clinical symptoms or other imaging studies (such as sonography or endoscopic cholangiopancreatography) who underwent multiphasic CT scanning of the pancreas using the dual-energy scanning mode of a dual-source CT scanner (SOMATOM® Definition Dual Source; Siemens Medical Solutions, Forchheim, Germany) between January 2009 and July 2010 were included in this study. All patients had focal pancreatic lesions. The pancreatic lesions were classified into three categories: cystic (n=19), solid hypovascular (n=21) and solid hypervascular (n=4). The final diagnosis and mass characterisation are summarised in Table 1. 75% (33/44) of final diagnoses were confirmed by surgical resection and percutaneous needle biopsy, and 25% (11/44) of the patients were diagnosed by characteristic features on endoscopic retrograde cholangiopancreatography or MR cholangiopancreatography (MRCP). There were eight cases of branch duct-type intraductal papillary mucinous neoplasms (IPMNs), four cases of main duct-type IPMNs and one case of mixed IPMNs. All patients had undergone routine protocol pancreatic CT scanning, which consisted of pre-contrast, early arterial, pancreatic and portal phase image sets with a conventional CT scanner, during the follow-up period. Early arterial phase images were obtained for evaluating the vascular anatomy and the presence of stenosis or occlusion in the coeliac and superior mesenteric arteries, and were used for creating three-dimensional CT angiography images.

The mean (±SD) weight for all patients was 60.9 ± 11.8 kg (range 41.55–87.00 kg), the mean ± SD height was 162.45 ± 8.70 cm (range 143.7–185.8 cm) and the mean ± SD body mass index (body mass index="" weight in kilograms divided by the square of height in metres) was 22.97 ± 3.36 kg m^{-2} (range 17.30–31.06 kg m^{-2}).

CT protocol

Scan protocol

Multiphasic pancreatic protocol CT scans composed of pre-contrast, early arterial, pancreatic and portal phase images were routinely obtained using the SOMATOM Definition dual-source CT scanner. The detailed DECT scanning parameters and post-processing algorithms are presented in Table 2. Iodinated contrast medium (iopromide, Ultravist® 370; Bayer-Schering, Berlin, Germany) at a dose of 1.5 cm^3 kg^{-1} (=555 mgI kg^{-1}) was injected at a rate of 3–5 ml s^{-1} for 30 s using a power injector (Stellant® Dual; Medrad, Indianola, PA) and was followed by injection of 30–40 ml of normal saline [13, 14]. CT scans were routinely obtained with the patient in a supine position during full inspiration. The scan range of the pre-contrast, early arterial and pancreatic phase images was from the lung base to the mid-pole of the kidney. Portal phase scanning covered the area from the lung base to the lower margin of the iliac crest. The arterial phase scan timing was determined using the CARE bolus technique (Siemens) [15]. Early arterial phase scanning was automatically started 6 s (minimum delay) after the attenuation coefficient of abdominal aortic blood reached 80 HU at 140 kVp (corresponding to 100 HU at 120 kVp). The mean scanning delays for the early arterial, pancreatic and portal phases were 26, 40 and 70 s, respectively. The automatic dose modulation protocol provided by the manufacturer (CARE Dose 4D; Siemens) was used as it adjusts tube current in a real-time manner in order to keep image noise at an optimal level [16]. The tube current of 80 kVp tube (340 mAs) was roughly four times that of the 140 kVp tube (80 mAs) in order to match the noise level to the greatest possible

Table 1. Mass characterisation and enhancement pattern with the final diagnosis of the study population

Mass characterisation		Final diagnosis	n	Confirmation	
				Pathological	Morphological
Solid	Solid hypovascular	Pancreatic adenocarcinoma	18	18	
		Solid pseudopapillary neoplasms	3	3	
	Solid hypervascular	Neuroendocrine tumour	4	4	
Cystic		Intraductal papillary mucinous neoplasms	13	4	9
		Mucinous cystadenoma	2	2	
		Pseudocyst	2		2
		Serous microcystic adenoma	1	1	
		Solid pseudopapillary neoplasms (cystic)	1	1	

Table 2. Dual-energy CT scanning parameters and post-processing

CT Scanning parameters	Pre-contrast	Early arterial	Pancreatic	Portal venous
Voltage (kVp)	120	80	Dual energy (80/140)	
Mean scanning delays after contrast injection (s)		26	40	70
Collimation (mm)	64×0.6		14×1.2	
Rotation time (s)	0.5		0.5	
Pitch	0.9		0.85	
Kernel	B30f		D30f	
Tube current (mAs)	150	210	80 (140 kVp tube) 340 (80 kVp tube)	

extent [10]. These tube currents were chosen so that the images created were approximately dose-matched compared with single-source CT acquisition at 120 kVp. For each of the four phases, the dose–length products, which were automatically calculated by an implemented program in the CT scanner, were recorded and used to calculate the individual, effective radiation dose using appropriately normalised conversion factors [17]. We also compared each patient's radiation dose on DECT scanning with that of the follow-up, routine and pancreatic CT scanning at fixed 120 kVp.

Image generation

Axial images of all phases were reconstructed at a slice thickness of 3 mm and a reconstruction interval of 2 mm. Three linear-blended images with different weighting factors (0.3, 0.5 and 0.7) for the low-voltage image (80 kVp), VNE images and iodine-only images were generated using a dedicated workstation for post-processing images of DECT data (Multi Modality Workplace; Siemens). A weighting factor of 0.3 means that the image was generated using a ratio of 0.3 of the 80 kVp image and 0.7 of the 120 kVp image. An iodine map to encode the iodine distribution in each individual CT voxel was generated and subsequently used to subtract iodine from the image, and was thus used in a VNE image. The VNE images were generated from portal venous phase scans. The standard, soft-tissue attenuations used by this system were 65 and 45 HU for 80 and 140 kVp, respectively, while the typical fat attenuations were –110 and –95 HU, respectively.

Image analysis

Qualitative analysis

Two abdominal radiologists (with 14 and 5 years, respectively, of clinical experience interpreting abdominal CT scans) independently assessed the six image sets. They were blinded to the pathology results, and analysis was performed using the stack mode of a picture archiving and communications workstation (PACS; Marotech, Seoul, Republic of Korea). The reviewers viewed each image set and changed the window and/or level settings according to their preference. Axial true non-enhanced (TNE) and VNE images were displayed side by side. The readers were not blinded as to which images represented the TNE or VNE data set as those images could easily be discriminated. For TNE and VNE images, the radiologists rated the overall image quality using a five-point scale as follows: 1, excellent; 2, good; 3, fair; 4, poor; 5, not interpretable. Based on their overall impression of the images, the radiologists were asked to decide whether VNE images could replace TNE images with a rating as follows: 1, completely; 2, with restrictions; 3, not acceptable. The readers also assessed the presence and type of artefacts on VNE images. They were asked to describe any added values of iodine-only images compared with the linear-blended image with a weighting factor of 0.3.

For three linear-blended image sets, the assessments were made without any information regarding the image-blending parameters. The reviewers ranked the images twice, from 1 (most preferred) to 3 (least preferred), according to the lesion conspicuity and overall image quality regarding lesion detection and characterisation. If the images were too similar to rate differently, the reviewers were permitted to give the same rates.

Quantitative analysis

On the TNE, VNE and the three linear-blended image sets, the 80 kVp and 140 kVp images' Hounsfield units and the SDs were measured by selecting regions of interest (ROIs) in the pancreatic lesion, as well as in five other anatomical regions (*i.e.* normal pancreatic parenchyma, liver parenchyma, abdominal aorta, psoas muscle and retroperitoneal fat). The mean ± SD ROI size was $96.6 \pm 18.0\,mm^2$ (range 9.6–134.1 mm^2) for pancreatic lesions and $100.70 \pm 10.42\,mm^2$ (57.2–109.4 mm^2) for other anatomical regions. The attenuation stability and image noise were determined by measuring the mean Hounsfield units and SD of the retroperitoneal fat. The signal-to-noise ratio (SNR) was calculated in the TNE and VNE images as $SNR = ROI_L/ROI_P$, where ROI_L is the mean attenuation value of the pancreatic lesion and ROI_P is the mean attenuation value of the normal pancreatic parenchyma. For each pancreatic lesion in the three linear-blended image sets, the lesion-to-pancreas CNR was calculated as $CNR = (ROI_L - ROI_P)/\sigma(ROI_{Rf})$, where $\sigma(ROI_{Rf})$ is the SD of the attenuation values of retroperitoneal fat [18].

Statistical methods

For qualitative analysis, arithmetic means and SDs were calculated for the overall image quality ranks and the results were tested for statistical significance using the Wilcoxon test. The frequency of each image rating category was also recorded. For quantitative analysis, the Hounsfield units measured on all images were summarised by calculating the arithmetic mean and the

corresponding standard deviation. Statistical significance was assessed using Student's *t*-test for paired samples to compare the TNE and VNE images, kappa statistics to evaluate interobserver agreement, repeated measures of analysis of variation with Bonferroni correction to compare quantitative analysis and the Friedman test to compare the qualitative analysis of the three linear-blended images. Effective radiation doses for CT protocols including or excluding the TNE images were compared using a paired *t*-test. A *p*-value <0.05 was considered to indicate a statistically significant difference. For statistical analysis, GraphPad™ (v. 3.05; InStat Software, San Diego, CA) and MedCalc™ (v. 11.1.1; MedCalc Software bvba, Mariakerke, Belgium) were used.

Results

Qualitative analysis

When comparing the TNE and VNE images, the TNE images scored better than the VNE images in terms of overall image quality, according to the reviewers ($p<0.0001$): the mean ± SD scores for the TNE images were 1.11 ± 0.32 (39 excellent, 5 good) and 1.05 ± 0.21 (42 excellent, 2 good) for Reviewers 1 and 2, respectively, whereas those for the VNE images were 2.00 ± 0.57 (7 excellent, 30 good, 7 fair) and 1.52 ± 0.51 (21 excellent, 23 good). In addition, 90.9% (80/88; 39/44 from Reviewer 1, 41/44 from Reviewer 2) of the VNE studies were rated as completely acceptable, with the remaining 8 studies rated as acceptable with restrictions. Artefacts of the VNE images were noted in 37/44 (84.1%) and 26/44 (59.1%) of the VNE images by Reviewers 1 and 2, respectively. These were subtraction, beam hardening, blurring and streak artefacts.

Regarding the iodine-only images, half (22/44 for each reviewer) of the cases were regarded as having an added diagnostic value for the evaluation of pancreatic disease. The major reasons for the added diagnostic values were a more accurate determination of the cystic or solid nature of a lesion, as well as greater lesion conspicuity and a clearer assessment of the relationship of the pancreatic duct to nearby vessels, such as the superior mesenteric artery or vein.

For the qualitative analysis of the reviewers' preference on three sets of linear-blended images, the images with a weighting factor of 0.7 were chosen as the most preferred image set for lesion conspicuity (76/119; $\kappa=0.464$). The linear-blended images with a weighting factor of 0.3 were most favoured regarding image noise (93/99; $\kappa=0.656$). The linear-blended images with a weighting factor of 0.5 were chosen by both reviewers as the best images, considering their overall image quality (55/107; $\kappa=0.313$). Figure 1 shows the number of cases in which each blending method was ranked as the best and as the least-preferred image set by both reviewers.

Quantitative analysis

The mean attenuation values of both the normal parenchyma and lesions in the pancreas, as well as the image noise and CNR in each image set, are shown in Table 3. When comparing TNE and VNE images, we did not observe a statistically significant difference in the mean attenuations of the pancreatic lesions ($p>0.05$) and mean attenuation values for normal pancreatic parenchyma ($p>0.05$). There were no significant differences in SNR values in the TNC and VNC images ($p=0.44$). The CNR value of the VNE images (mean=2.27) was statistically higher than that of the TNE images (mean=1.14; $p<0.0001$). Image noise was significantly lower in VNE (9.89 ± 3.94) than in TNE (15.43 ± 5.02) images ($p<0.0001$). These results could be artificial, affected by smoothing filters implemented in the software which was used in VNE image generation. In mixed image sets, the mean attenuation values of all measured lesions showed a significant increase as the weighting factor increased. The CNR value of the weighting factor of 0.3 was better than that of the other image sets, with statistical significance only in the cystic group ($p=0.0325$) and the solid hypovascular group ($p=0.0333$). However, there was no significant difference in CNR values among the three weighted images in patients with whole solid tumours ($p>0.05$).

Radiation dose

The mean effective dose in the TNE phase was 1.36 ± 0.25 mSv (minimum 0.975 mSv, maximum 2.025 mSv). In addition, the mean effective doses of the late arterial phase in DECT and routine fixed 120 kVp CT scans were 2.84 mSv and 3.45 mSv, respectively. If we exclude TNE images from the dual-energy scanning protocol, the radiation dose in the early arterial, pancreatic and portal phases was 8.29 mSv, which was significantly lower than the value of each patient's follow-up, routine pancreatic protocol CT using 120 kVp (mean ± SD 13.94 ± 2.82 mSv). The radiation dose percentage of the TNE images compared with the radiation dose of the total image scan protocol was 14.14% (1.36/9.65 mSv).

Discussion

In our study, DECT was able to provide high-quality VNE images that could replace TNE images in more than 90% of our study population, and iodine-only images that showed an added value in 50% (44/88) by improving differentiation between the cystic or solid nature of the

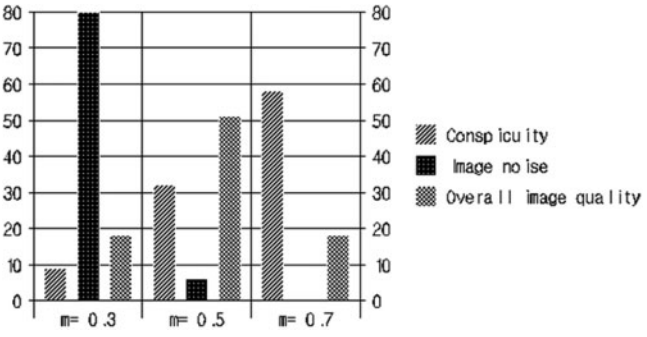

Figure 1. The number of most preferred images of the mixed image sets regarding lesion conspicuity, image noise, and overall image quality.

Table 3. Mean Hounsfield units, image noise and contrast-to-noise ratio (CNR) measured on three linear mixed image sets, and on 80 and 140 kVp images

	TNE	VNE	140 kVp	Weighting factor			80 kVp	*p*-value
				0.3	0.5	0.7		
Hounsfield units								
Normal pancreas	38.9 ± 9.7	36.9 ± 11.6	107.6 ± 14.6	123.0 ± 20.2	137.0 ± 20.1	151.2 ± 25.8	187.9 ± 24.3	
Lesion (cystic, n=19)	14.7 ± 10.5	9.5 ± 18.8	33.9 ± 51.0	37.9 ± 56.6	43.3 ± 68.0	43.5 ± 69.3	54.5 ± 84.8	
Lesion (solid, n=25)	33.4 ± 14.2	32.7 ± 14.7	59.0 ± 41.1	70.1 ± 44.8	83.9 ± 48.3	93.2 ± 56.4	105.1 ± 75.4	
Hypovascular (n=21)	30.0 ± 9.0	28.9 ± 11.6	45.8 ± 19.8	56.3 ± 22.4	67.7 ± 23.4	73.3 ± 24.7	77.5 ± 28.7	
Hypervascular (n=4)	39.1 ± 0.5	41.7 ± 6.5	128.3 ± 57.1	142.0 ± 64.9	164.6 ± 65.7	185.5 ± 79.6	233.4 ± 104.2	
Image noise[a]				12.8 ± 3.6	15.4 ± 3.5	17.0 ± 3.6		<0.0001[b]
CNR (cystic, n=19)				8.0 ± 2.6	7.6 ± 2.5	7.3 ± 1.9		0.0325[b]
CNR (solid, n=25)				5.6 ± 3.0	5.2 ± 2.6	4.8 ± 3.1		>0.05[b]
Hypovascular (n=21)				6.3 ± 3.7	5.6 ± 2.7	5.3 ± 3.3		0.0333
Hypervascular (n=4)				4.4 ± 2.4	3.5 ± 2.0	3.7 ± 2.4		0.1132

TNE, true non-enhanced; VNE, virtual non-enhanced.
[a]Image noise refers to standard deviations of the retroperitoneal fat, $CNR=(ROI_L-ROI_P)/\sigma(ROI_{Rf})$, where ROI_L is the mean attenuation value of the pancreatic lesion, ROI_P is the mean attenuation value of the normal pancreatic parenchyma and $\sigma(ROI_{Rf})$ is the standard deviation of attenuation values of retroperitoneal fat.
[b]*p*-value comparing each value from the images with weighting factor 0.3 *vs* 0.5, 0.5 *vs* 0.7, 0.3 *vs* 0.7.

lesions or improving lesion conspicuity (Figures 2–4). Our study results are consistent with those of earlier studies, which suggested that iodine-only images may provide information regarding contrast material distribution in intra-abdominal solid organs [10, 19]. The advantage of the iodine-only images for differentiating cystic lesions from solid lesions was attributed to the higher sensitivity of low-kVp scanning data regarding iodine, as the solid portion shows enhancement after administration of iodinated contrast medium. The lesions that showed better conspicuity on iodine maps were pancreatic cancer (Reviewer 1=6, Reviewer 2=6) and one case of branch duct IPMN (both reviewers agreed). The increased conspicuity is possibly due to the hypovascular nature of pancreatic cancer and the IPMN, both of which result in more exaggerated low attenuation than that seen in normal pancreatic parenchyma on iodine maps.

In our study, VNE images were acceptable as an alternative to TNE images >90% of the time for pancreatic disease evaluation (80/88), and showed no statistically significant difference in the SNR compared with the TNE image sets ($p>0.05$). Moreover, the CNR was significantly higher in VNE images, and VNE images showed lower noise than TNE images, which was attributed to the noise reduction filter. Our results agreed with those of several previous studies in patients after endovascular aneurysm repair, patients with renal and adrenal masses, and patients with liver parenchymal lesions [19–22], demonstrating a comparable image quality of VNE images to that of TNE images. Therefore, if we omitted the acquisition of TNE images from our pancreatic protocol CT imaging, which was composed of pre-contrast, pancreatic and hepatic venous phase images, we could reduce approximately 14.14% (mean=1.36 mSv) of the total radiation dose of our routine pancreatic protocol CT imaging (mean=9.65 mSv). Although there were still a few problems with VNE, including artefacts due to inhomogeneous mixing or inadequate breath-holding, smaller size of calcifications, and limited field of view (26 cm), the problem of limited field of view has lessened with the second-generation DECT scanner.

In addition, in our study the reviewers showed a strong preference for linear-blended images with a weighting factor of 0.5 compared with linear-blended images with weighting factors of 0.3 and 0.7. We believe that this could be attributed to the fact that the reviewers tended to prefer images with higher contrast at the expense of high noise rather than intermediate contrast with intermediate noise or low contrast with low noise among the image sets with similar CNR values, especially for detecting small, subtle, hypo-attenuated pancreatic lesions [23]. For the subjective analyses of the CT examinations, linear-blended images with a weighting factor of 0.3 were least preferred by the reviewers. But in objective analyses, the weighting factor of 0.3 showed the best CNR value among the three image sets. The differences in CNR between the images with a weighting factor of 0.3 and the images with a weighting factor of 0.5 or 0.7 were statistically significant among the cystic lesions and solid hypovascular tumours ($p<0.05$). However, in analysis of all solid tumours (n=25), the CNR value indicated a preference for images with a weighting factor of 0.3, but failed to demonstrate statistical significance ($p>0.05$). These results may be

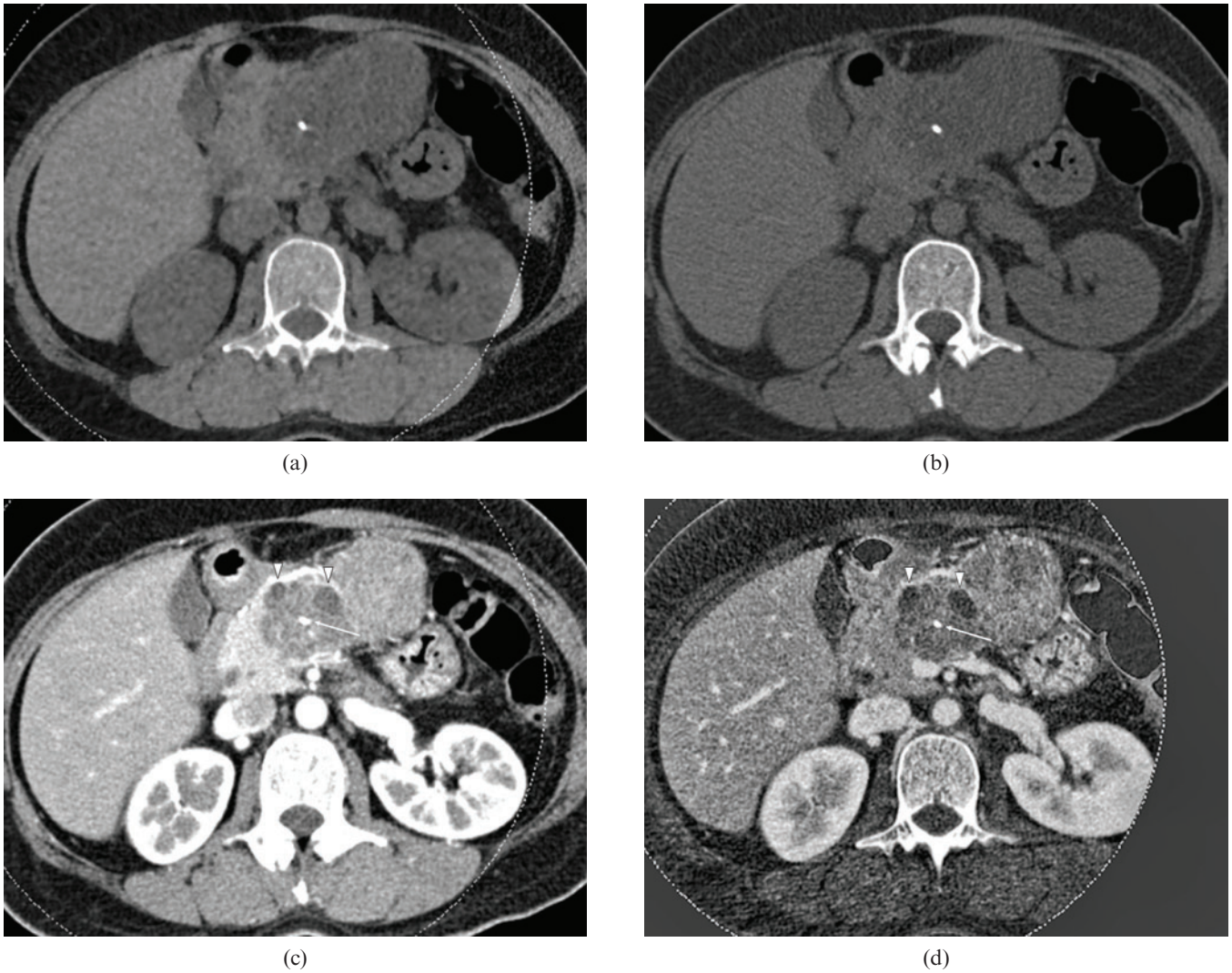

Figure 2. 48-year-old female with serous cyst adenoma of the pancreas. (a) Virtual non-enhanced image shows comparable image quality to the (b) true non-enhanced image. (c) Mixed image with a weight factor of 0.3 shows a multilobulated solid mass with a suspicious internal low-attenuation portion (arrow heads) and calcification (arrow). However, it is not certain whether the low attenuated portions are cystic or solid component. (d) In the iodine map, those areas appear more likely to be of low attenuation, thus highly suggesting their cystic nature. There is calcification in the center of the mass (arrow).

due to the difference in attenuation values between the normal pancreas and pancreatic mass. In hypervascular tumours, the contrast between pancreatic parenchymal tissue and mass was lower than that between pancreas and hypovascular mass. Our results are not consistent with a recent study of patients with pancreatic adenocarcinoma [18], which reported that the CNR was significantly higher at 80 than at 120 kVp and other

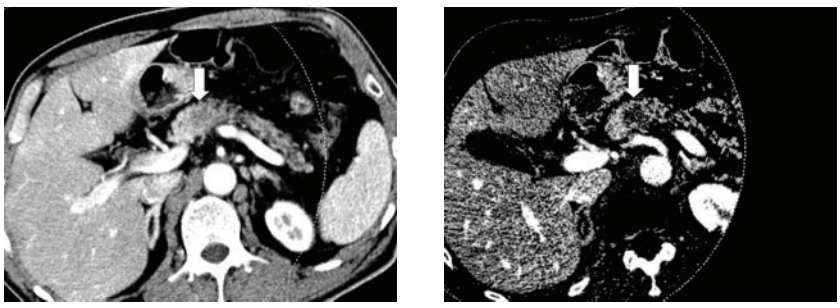

Figure 3. 55-year-old male with pancreas body adenocarcinoma. (a) The axial CT scan with a weight factor 0.3 shows an ill–defined, low-attenuation lesion (arrow) in the pancreas body. (b) The iodine map shows much better lesion conspicuity compared with the mixed image, due to the higher lesion-to-pancreas contrast.

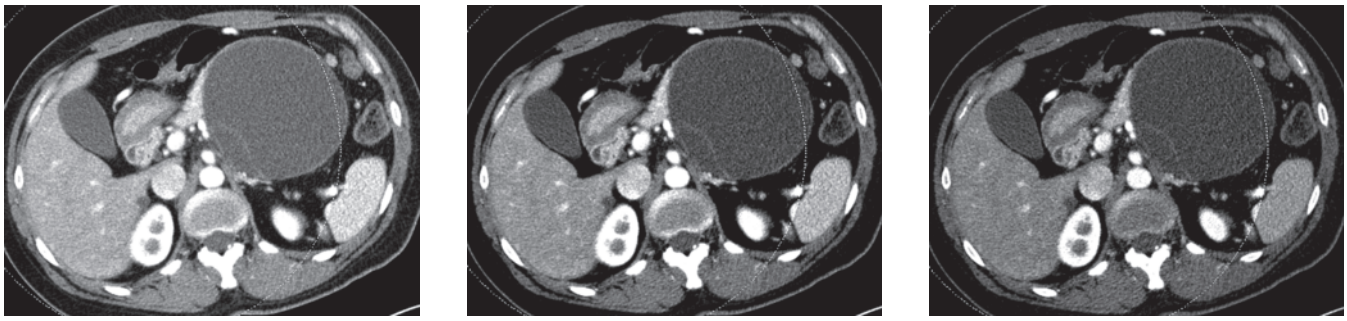

(a) (b) (c)

Figure 4. 40-year-old female with mucinous cystic adenoma. Dual-energy CT images with a weight factor of (a) 0.3, (b) 0.5, and (c) 0.7, all show a large, cystic mass with the thin wall as well as internal septation in the pancreas tail. The image with a weight factor of 0.3 shows the least noise, although the septation is better visualised as internal septation is on the weight factor 0.7 image. Note that the internal cystic component appears to be coarse on the image with weight factor 0.7. The image with weight factor 0.5 shows relatively higher contrast than the image with weight factor 0.3 and lower noise than the images with weight factor 0.7. Both reviewers selected image (b) as the preferred image.

weighted-average peak kilovoltage images. Similar to the previous study, our study also demonstrated that the attenuation difference between the lesions and normal pancreatic parenchymal tissue showed an increasing difference according to an increasing ratio of the weighting factor. However, in our study, the CNR value was higher in the least weighted (weighting factor 0.3) image set than in the other mixed image sets. We believe that the discrepancy between the previous study and our study could be attributed to the different patient population with a different body habitus (body mass index). We calculated the CNR value as $(ROI_L - ROI_P)/\sigma(ROI_{Rf})$. Therefore, we can assume that $\sigma(ROI_{Rf})$, which represents image noise, was significantly lower in the weighting factor of 0.3 image sets, which compensated for the decrement of the attenuation difference compared with the linear-blended images with the increasing ratio of the weighting factor.

There were several limitations in our study. First, a major limitation is its retrospective nature, which resulted in our limited control regarding patient selection. Second, the study patient number was relatively small. Third, there were several lesions that were not pathologically diagnosed. Fourth, our study showed some variability according to the preference of the reviewers. This finding might suggest that the acceptance level of noise or lesion conspicuity standards were not the same for each reviewer. Further study will be required with a larger patient population to determine the optimal reconstruction parameters for detecting pancreatic lesions.

In conclusion, DECT has the potential to provide an added diagnostic value for evaluation of focal pancreatic tumours by providing VNE images that could replace TNE images, and may reduce radiation dose and the iodine map, improving differentiation between the cystic or solid nature of the lesions, or improving lesion conspicuity compared with simulated weighted 120 kVp images.

References

1. Horton KM. Multidetector CT and three-dimensional imaging of the pancreas: state of the art. J Gastrointest Surg 2002;6:126–8.
2. Paspulati RM. Multidetector CT of the pancreas. Radiol Clin North Am 2005;43:999–1020, viii..
3. Tsiotos GG, Farnell MB, Sarr MG. Are the results of pancreatectomy for pancreatic cancer improving? World J Surgery 1999;23:913–19.
4. Beger HG, Rau B, Gansauge F, Poch B, Link KH. Treatment of pancreatic cancer: challenge of the facts. World J Surgery 2003;27:1075–84.
5. Hanbidge AE. Cancer of the pancreas: the best image for early detection—CT, MRI, PET or US? Can J Gastroenterol 2002;16:101–5.
6. Brooks RA. A quantitative theory of the Hounsfield unit and its application to dual energy scanning. J Comput Assist Tomogr 1977;1:487–93.
7. Nakayama Y, Awai K, Funama Y, Hatemura M, Imuta M, Nakaura T, et al. Abdominal CT with low tube voltage: preliminary observations about radiation dose, contrast enhancement, image quality, and noise. Radiology 2005;237: 945–51.
8. Fletcher JG, Takahashi N, Hartman R, Guimaraes L, Huprich JE, Hough DM, et al. Dual-energy and dual-source CT: is there a role in the abdomen and pelvis? Radiol Clin North Am 2009;47:41–57.
9. Johnson TRC, Nikolaou K, Wintersperger BJ, Leber AW, von Ziegler F, Rist C, et al. Dual-source CT cardiac imaging: initial experience. Eur Radiol 2006;16:1409–15.
10. Graser A, Johnson TR, Chandarana H, Macari M. Dual energy CT: preliminary observations and potential clinical applications in the abdomen. Eur Radiol 2009;19:13–23.
11. Holmes DR 3rd, Fletcher JG, Apel A, Huprich JE, Siddiki H, Hough DM, et al. Evaluation of non-linear blending in dual-energy computed tomography. Eur J Radiol 2008;68: 409–13.
12. Behrendt FF, Schmidt B, Plumhans C, Keil S, Woodruff SG, Ackermann D, et al. Image fusion in dual energy computed tomography: effect on contrast enhancement, signal-to-noise ratio and image quality in computed tomography angiography. Invest Radiol 2009;44:1–6.
13. Goshima S, Kanematsu M, Kondo H, Yokoyama R, Miyoshi T, Kato H, et al. Pancreas: optimal scan delay for contrast-enhanced multi-detector row CT. Radiology 2006;241: 167–74.
14. Yanaga Y, Awai K, Nakayama Y, Nakaura T, Tamura Y, Hatemura M, et al. Pancreas: patient body weight tailored contrast material injection protocol versus fixed dose protocol at dynamic CT. Radiology 2007;245:475–82.
15. Kondo H, Kanematsu M, Goshima S, Miyoshi T, Shiratori Y, Onozuka M, et al. MDCT of the pancreas: optimizing scanning delay with a bolus-tracking technique for pancreatic, peripancreatic vascular, and hepatic contrast enhancement. AJR Am J Roentgenol 2007;188:751–6.

16. Graser A, Wintersperger BJ, Suess C, Reiser MF, Becker CR. Dose reduction and image quality in MDCT colonography using tube current modulation. AJR Am J Roentgenol 2006;187:695–701.
17. European Commission. European guidelines on quality criteria for computed tomography: EUR 16262. 2000. [Cited 24 August 2007]. Available from: http://www.drs.dk/guidelines/ct/quality
18. Macari M, Spieler B, Kim D, Graser A, Megibow AJ, Babb J, et al. Dual-source dual-energy MDCT of pancreatic adenocarcinoma: initial observations with data generated at 80 kVp and at simulated weighted-average 120 kVp. AJR Am J Roentgenol 2010;194:W27–32.
19. Yeh BM, Shepherd JA, Wang ZJ, Teh HS, Hartman RP, Prevrhal S. Dual-energy and low-kVp CT in the abdomen. AJR Am J Roentgenol 2009;193:47–54.
20. Zhang LJ, Peng J, Wu SY, Wang ZJ, Wu XS, Zhou CS, et al. Liver virtual non-enhanced CT with dual-source, dual-energy CT: a preliminary study. Eur Radiol 2010;20:2257–64.
21. Sommer WH, Graser A, Becker CR, Clevert DA, Reiser MF, Nikolaou K, et al. Image quality of virtual noncontrast images derived from dual-energy CT angiography after endovascular aneurysm repair. J Vasc Interv Radiol 2010;21:315–21.
22. Scheffel H, Stolzmann P, Frauenfelder T, Schertler T, Desbiolles L, Leschka S, et al. Dual-energy contrast-enhanced computed tomography for the detection of urinary stone disease. Invest Radiol 2007;42:823–9.
23. Gould RG, Belanger B, Goldberg HI, Moss A. Objective performance measurements versus perceived image quality in intensified fluoroscopic or photospot images. Radiology 1980;137:783–8.